SUPPORTING INFORMATION

Direct CO_2 Capture and Conversion to Fuels on Magnesium Nanoparticles at Ambient Conditions Simply Using Water

Sushma A. Rawool,[1] Rajesh Belgamwar,[1] Rajkumar Jana,[2] Ayan Maity,[1] Ankit Bhumla,[1] Nevzat Yigit,[3] Ayan Datta,[2] Günther Rupprechter,[3] Vivek Polshettiwar,[1]*

[1]Department of Chemical Sciences, Tata Institute of Fundamental Research (TIFR), Mumbai, India.
[2]School of Chemical Sciences, Indian Association for the Cultivation of Science, Kolkata, India.
[3]Institute of Materials Chemistry, Technische Universität Wien, Getreidemarkt 9/BC/165, 1060, Vienna, Austria.
Email: vivekpol@tifr.res.in, Phone: (91) 8452886556

Detailed procedure for liquid product analysis by ^{1}H NMR spectroscopy: The reaction was carried out in 5 ml of water and after completion of the reaction, the solution was recovered and centrifuged to separate the supernatant solution and solid residue. The supernatant aqueous solution was directly analyzed (for quantification, 0.5 mL of the supernatant solution and 60 µL of D_2O was mixed) by ^{1}H NMR (using water suppression pulse sequence). Quantification was carried out using the standard calibration curve.

Detailed procedure for gas product analysis by GC and GC-MS: The online monitoring of the gaseous products during the reactions as carried out using Micro GC (Agilent Technologies 490 Micro GC) directly connected to the reactor, using thermal conductivity detector (TCD), molecular-sieve column and argon as carrier gas. The gaseous products of the labeled $^{13}CO_2$ experiment were analyzed off-line by gas chromatograph equipped with TCD, flame ionization detector (FID) and mass spectrometer (MS) (Agilent 7890B, Agilent Technologies), Agilent hybrid column CP7430 and helium as carrier gas.

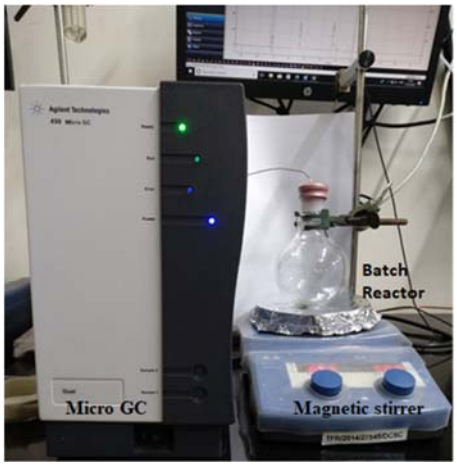

Experimental setup for Mg-assisted CO_2 conversion. The gaseous product of the reaction was identified and quantified using online microGC, offline GCMS and liquid product by ^{1}H NMR.

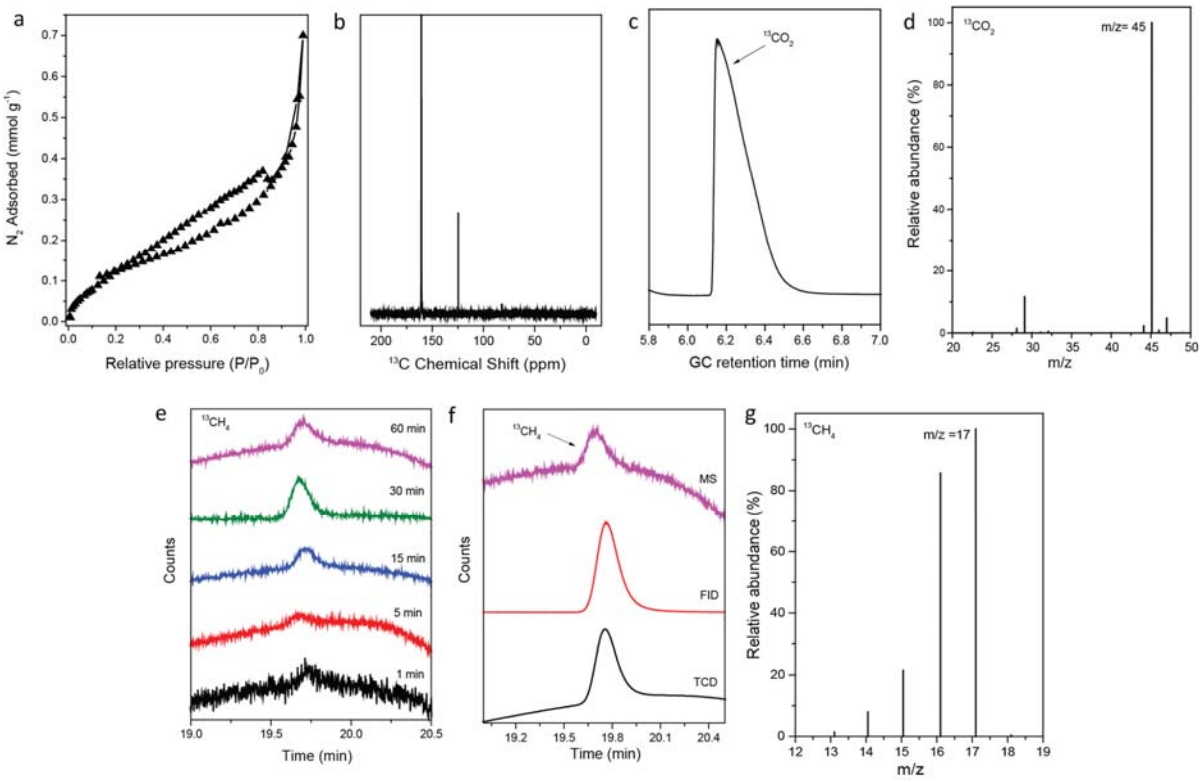

Figure S1. (a) N_2 sorption isotherm of Mg NPs; (b) ^{13}C NMR spectrum of the reaction mixture after 1 h of reaction using unlabeled CO_2, under exactly the same NMR pulse sequence and total number of scans (that of the $^{13}CO_2$ experiment). (c) gas chromatogram of CO_2 (peak of CO_2 at retention time 6.2 min), (d) mass spectrum of $^{13}CO_2$ (m/z = 45) (e) GC-MS recorded (peak of methane at retention time 19.7 min) with increasing reaction time, (f) Gas chromatogram recorded at 60 min with thermal conductivity detector (TCD), flame ionization detector (FID) and mass spectrometer (MS), (g) MS spectrum of isotopic $^{13}CH_4$ (m/z = 17) obtained at 60 min. For this, 50 mg of Mg NPs was taken in a 50 ml round bottom flask, and then $^{13}CO_2$ was purged through it for 1 min with a flow of 60 ml/min. The flask RB was evacuated and again $^{13}CO_2$ was passed through it for 1 min. Then, 5 ml water were added and the reaction products were monitored at 0, 1, 5, 15, 30 and 60 min, using a GC coupled with a TCD, FID and MS. The mass spectrum of the product methane showed the formation of isotopically labelled $^{13}CH_4$ (m/z = 17) by reduction of $^{13}CO_2$ gas.

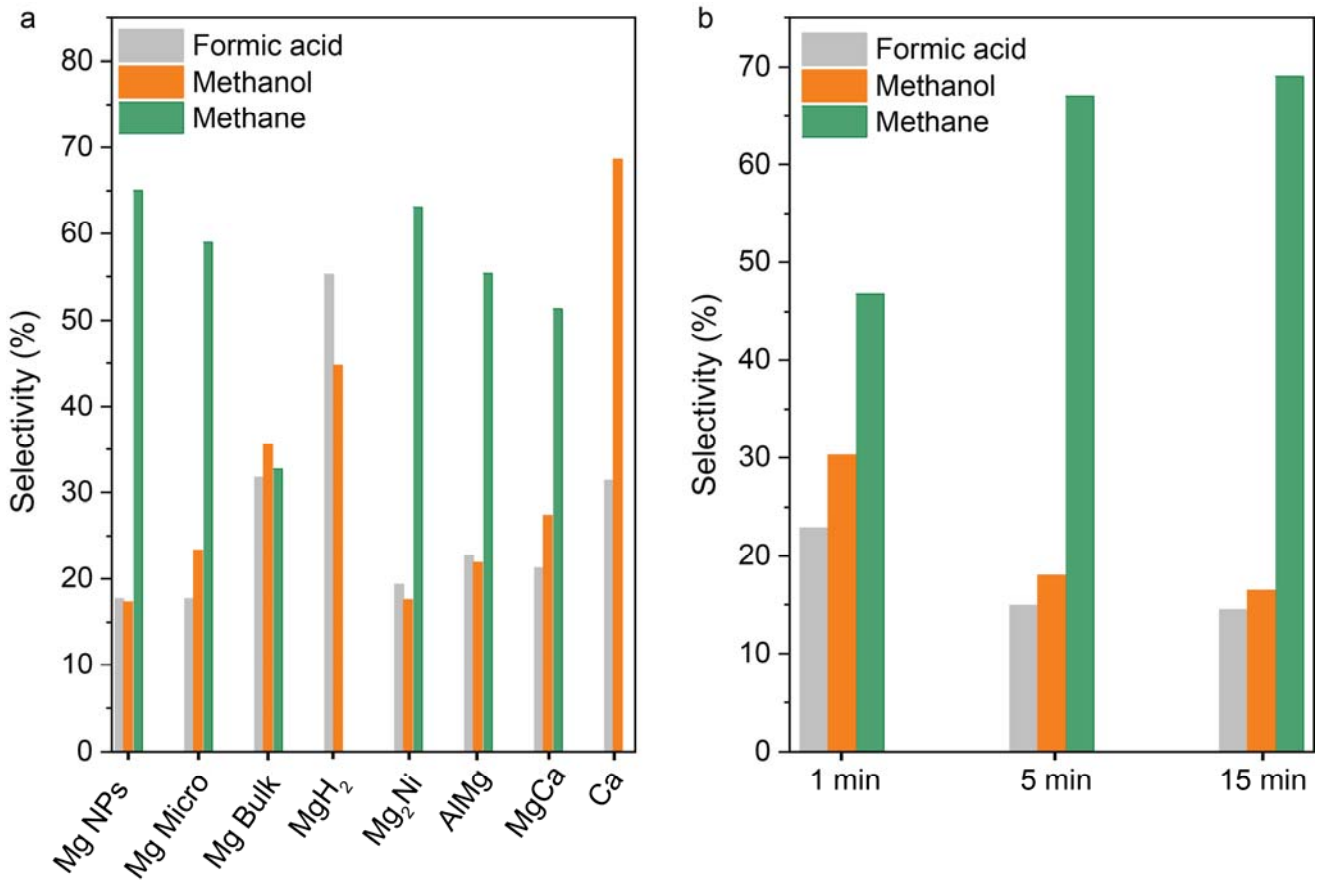

Figure S2. The selectivity of carbon-containing products (methanol, methane, and formic acid), using a) Mg and Mg alloy, b) Mg nanoparticles at various reaction time points, at room temperature and atmospheric pressure in water.

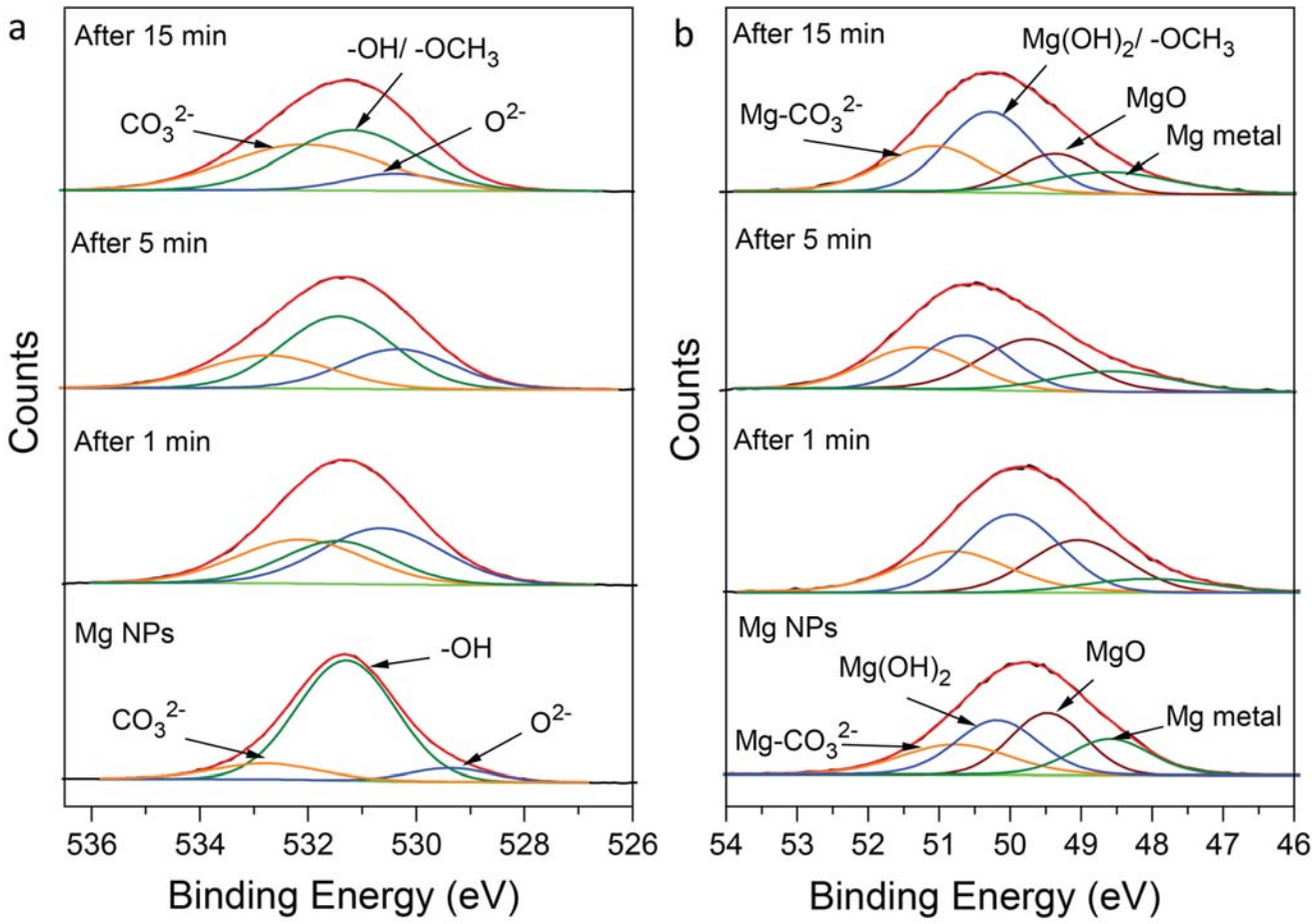

Figure S3. XPS spectra of (a) O 1s and (b) Mg 2p of Mg NPs and the solid product recovered after 1, 5 and 15 min of reaction time.

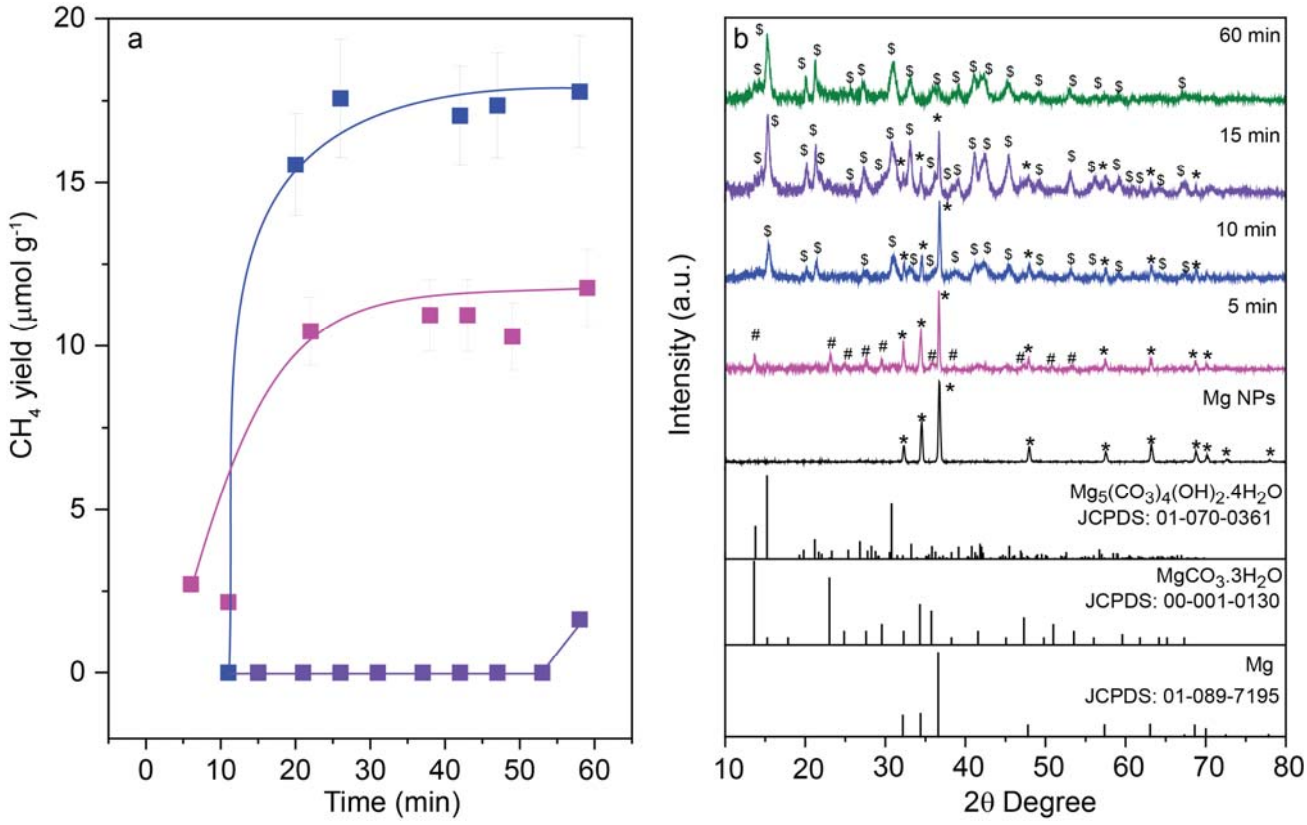

Figure S4. (a) Methane yield with reaction time from the reduction of CO_2 at room temperature and ambient pressure, using Mg NPs after initial products formed were flushed out after 5, 10, and 15 min of reaction. (b) PXRD patterns of the dried solid reaction mixture after 0, 5, 10, 15 and 60 min of reaction. Standard XRD patterns of Mg (JCPDS no.:01-089-7195), $MgCO_3.3H_2O$ (JCPDS No.:00-001-0130) and $Mg_5(CO_3)_4(OH)_2.4H_2O$ (JCPDS No.:01-070-0361) are also shown. (*Mg metal, $^{\#}MgCO_3.3H_2O$ and $^{\$}Mg_5(CO_3)_4(OH)_2.4H_2O$))

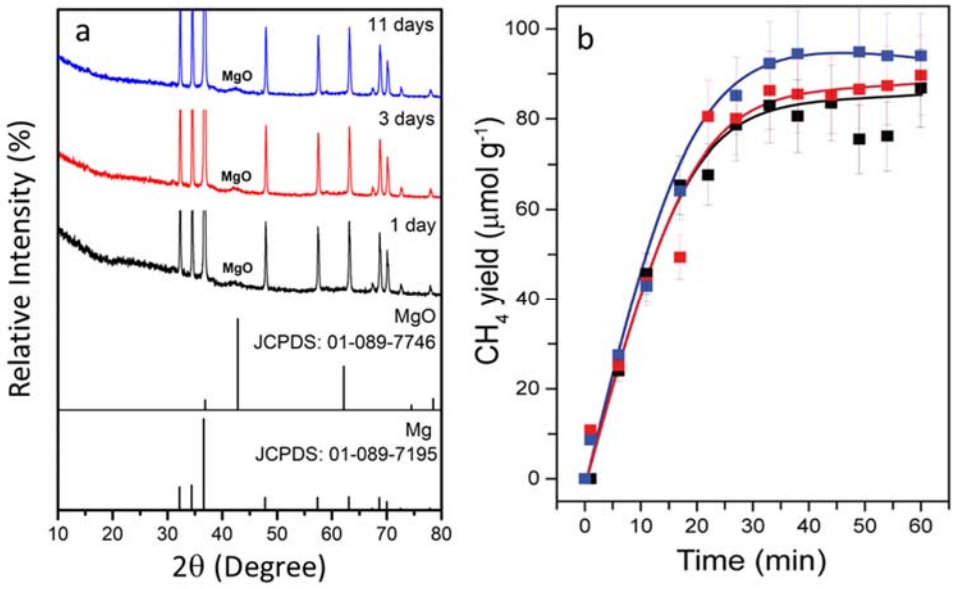

Figure S5. (a) PXRD pattern of Mg nanoparticles exposed to air 1, 3 and 11 days and standard patterns of Mg (JCPDS No.:01-089-7195) and MgO (JCPDS No.:01-089-7746), (b) methane yield with reaction time by reduction of CO_2 using water at room temperature and atmospheric pressure, using magnesium nanoparticles, exposed to air for 1, 3 and 11 days. Black- 1 day, Red- 3 days, Blue- 11 days. A weak PXRD peak indicated a thin MgO shell.

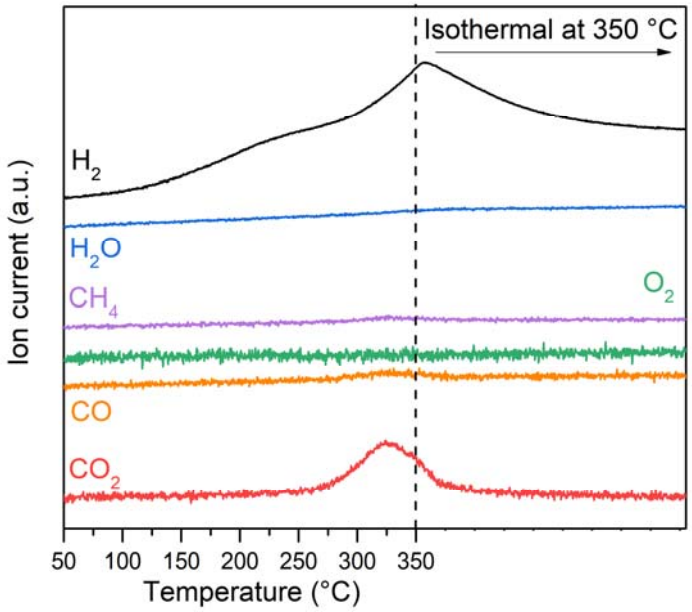

Figure S6. TPD-MS: To obtain clean surfaces, Mg NPs were pretreated at 350 °C in helium flow (heating rate 10 °C/min) before in situ ATR-FTIR studies. TPD-MS profiles revealed desorption of hydrogen (150-350 °C) and CO_2 (250-350 °C), resulting from the decomposition of bicarbonates on the Mg metal surface.

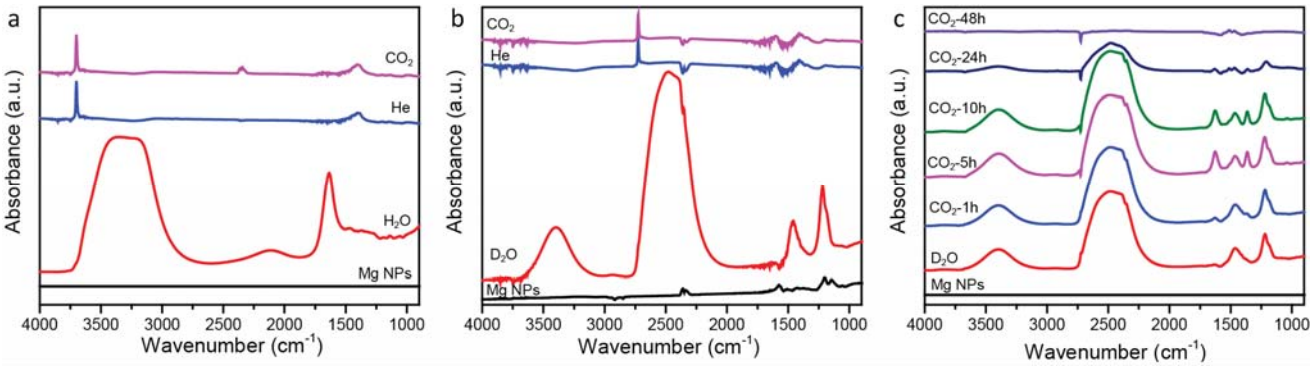

Figure S7. In situ ATR-FTIR spectra recorded (a) by adding (liquid) H_2O to the Mg NPs and subsequently purging with He and CO_2 gas, (b) by replacing H_2O with D_2O and subsequently purging with He and CO_2 gas, (c) by adding D_2O to the Mg NPs and then purging with CO_2 for 1, 5, 10, 24 and 48 h.

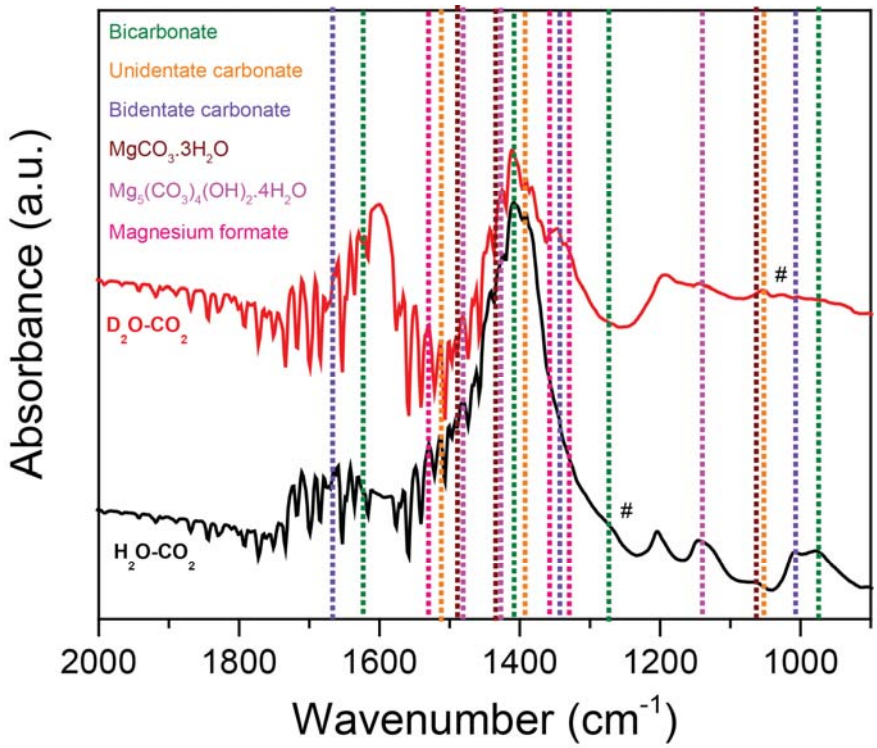

Figure S8. Comparison of ATR spectra recorded after passing CO_2 over Mg NPs treated with H_2O and D_2O, respectively. The absorption band at 1273 cm^{-1} of the C-OH bending mode of bicarbonate appeared at lower frequency 1024 cm^{-1} (marked as #).

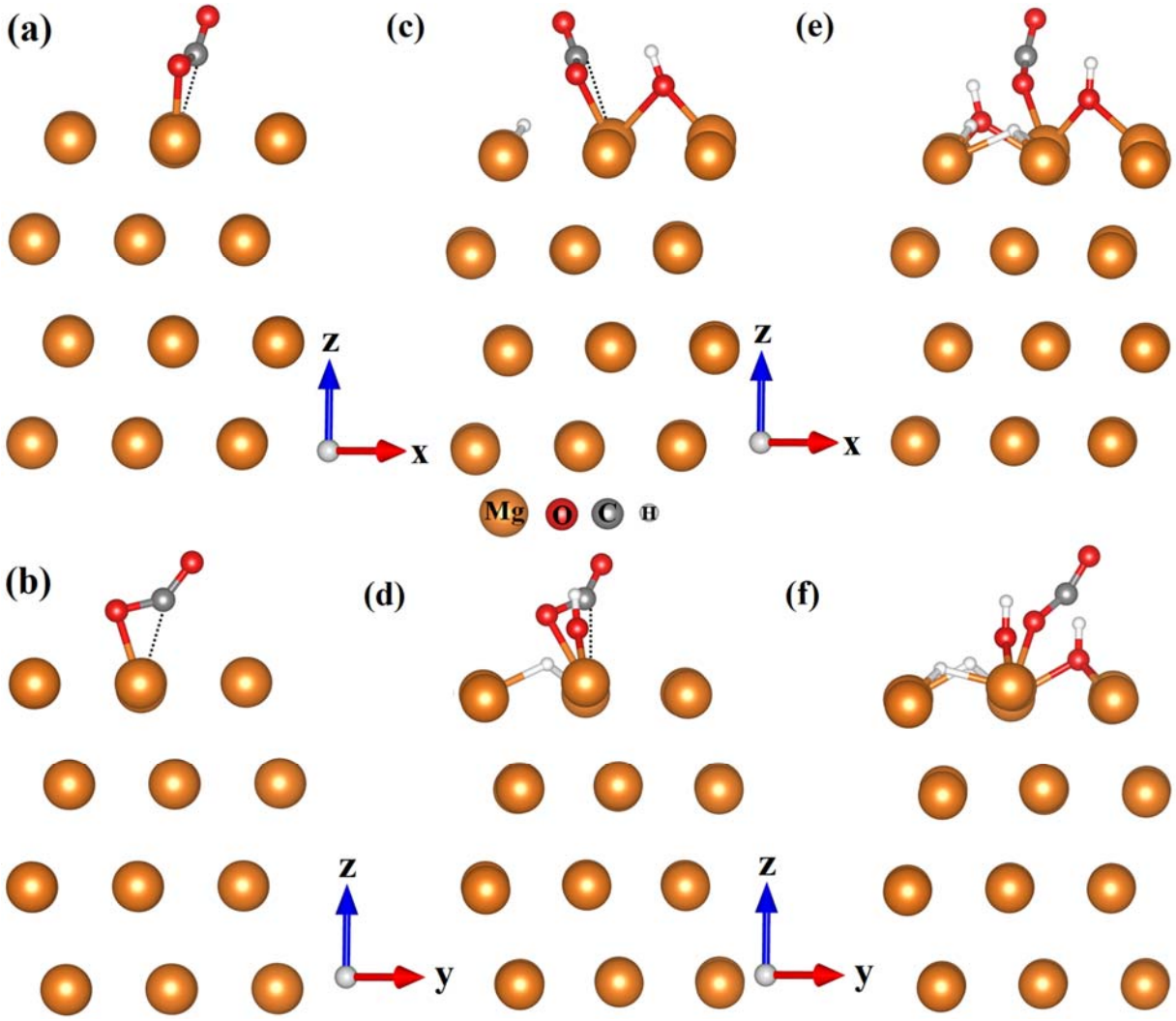

Figure S9. Different views of CO_2 adsorbed on the Mg surface: (a-b) adsorption on pristine Mg surface, (c-d) adsorption on hydrated Mg surface, (e-f) adsorption on $Mg(OH)_2$ surface (black dotted lines indicate weak interaction between carbon atom of CO_2 and surface Mg atom).

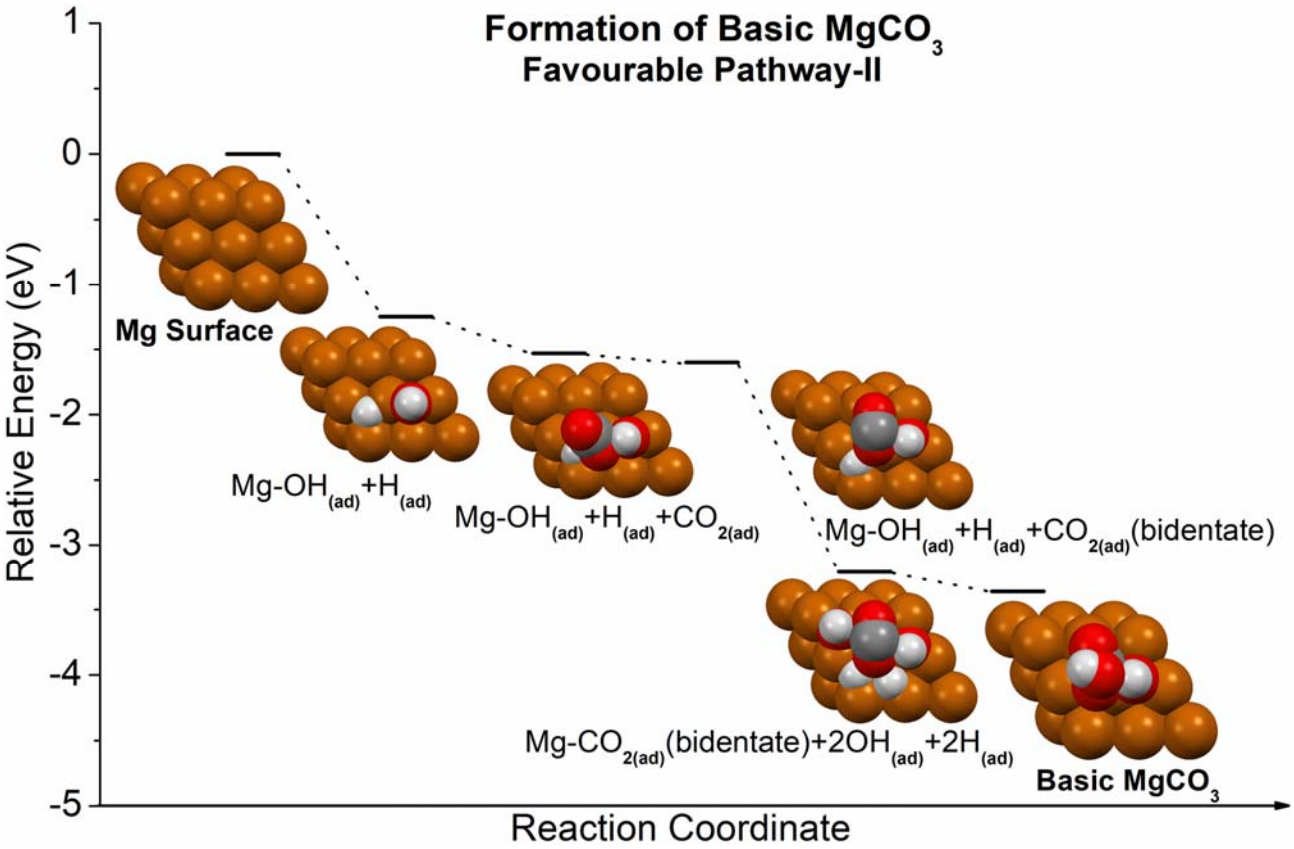

Figure S10. Potential energy surface of the formation of basic $MgCO_3$ via pathway-II.

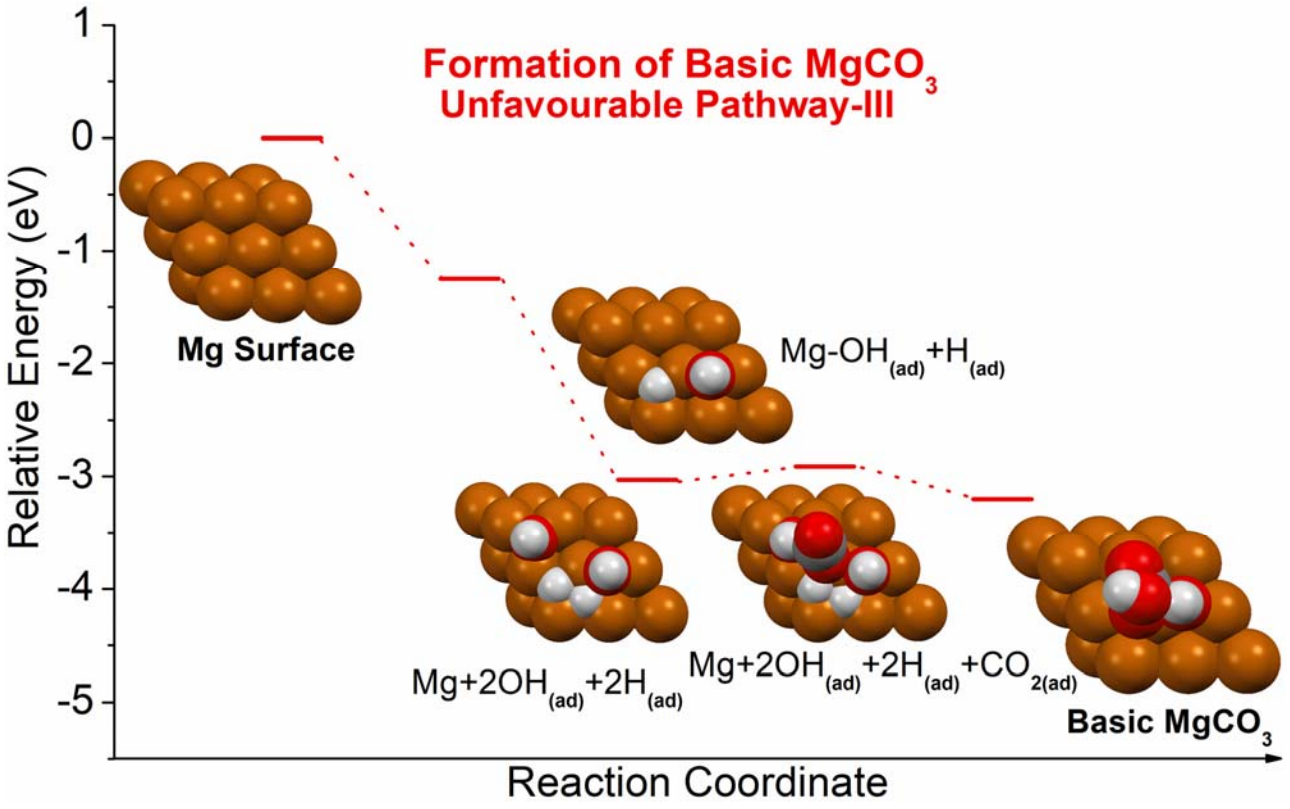

Figure S11. Potential energy surface of the formation of basic $MgCO_3$ via pathway-III.

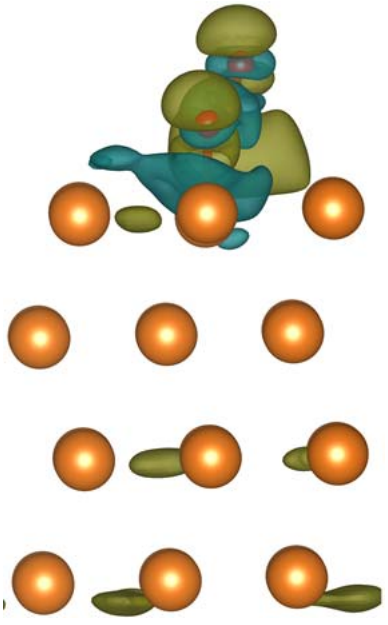

Figure S12. Charge density difference (CDD) plot (isodensity value at surfaces is ±0.002 e/au^3 (Positive: olive and Negative: cyan)) of CO_2 adsorbed on the pristine Mg surface, showing charge transfer in the region between CO_2 and surface atoms upon adsorption of CO_2.

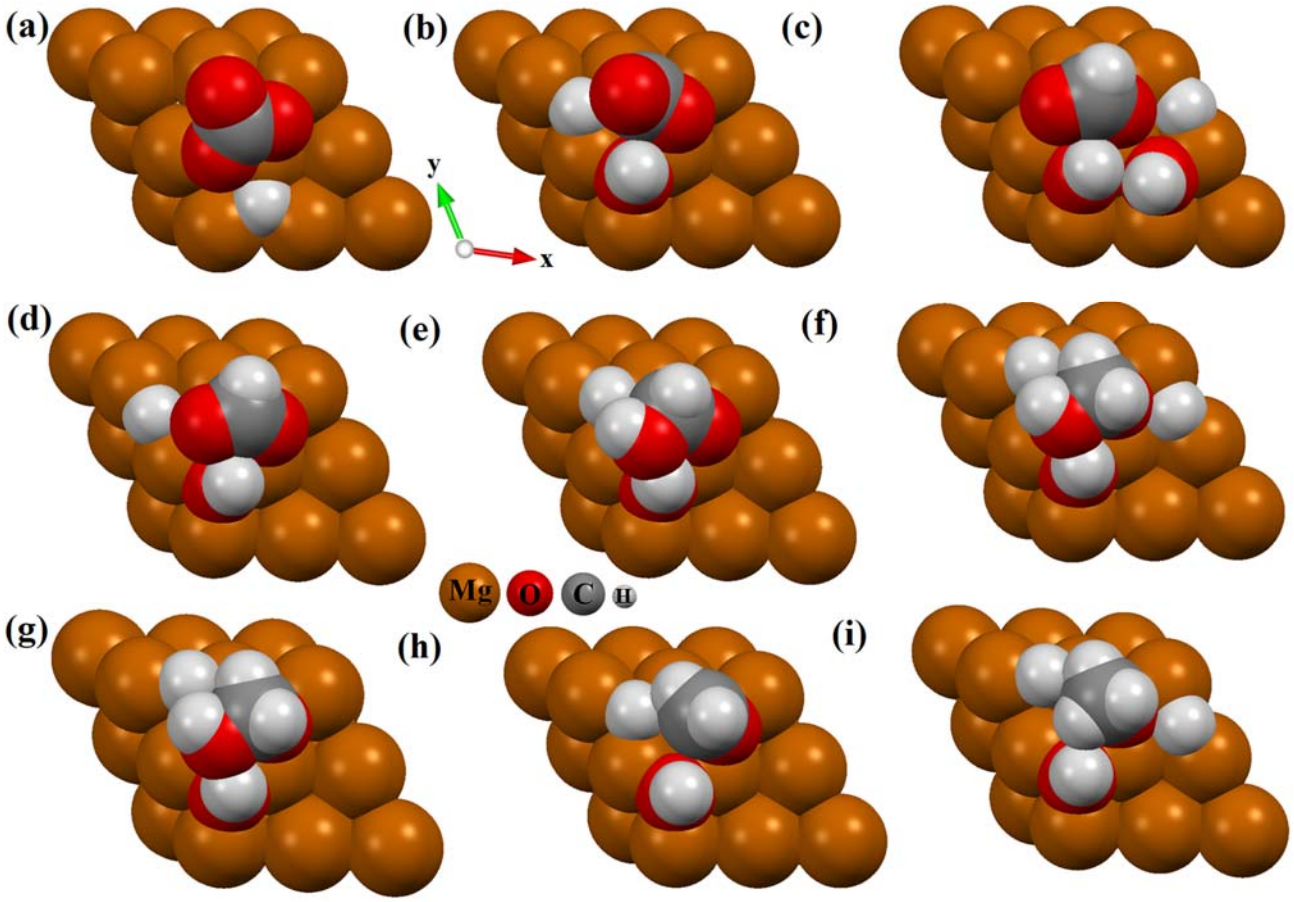

Figure S13. Structures of different intermediates for CO_2 to CH_4 formation: (a-i) represent the corresponding intermediate from intermediate A to I in figure 5.

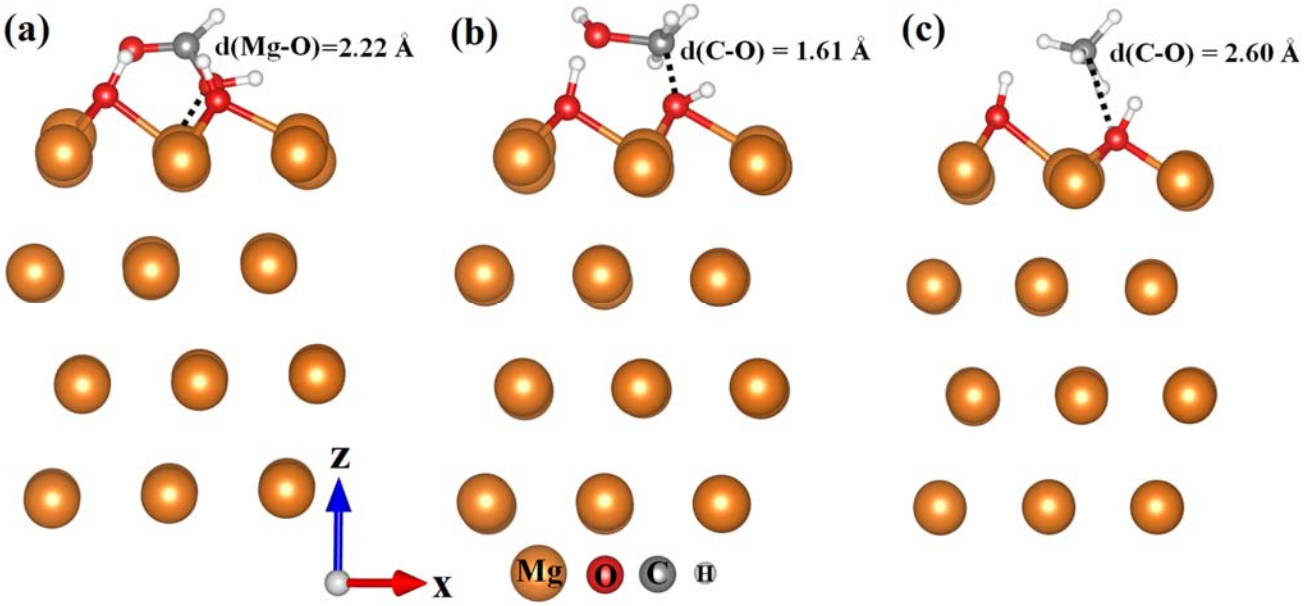

Figure S14. (a) HCOOH, (b) CH_3OH and (c) CH_4 adsorbed on the Mg surface during CO_2 reduction.

Mg Process Sustainability: The crucial magnesium electrolysis step to produce magnesium from Mg^{2+} requires low energy, and this process is highly efficient in industrial magnesium production from sea salts, with Faradaic efficiencies approaching 90%.[1] In comparison to other metals that convert CO_2 to chemicals and fuels, magnesium needs the lowest energy for production. For example,. Mg needs 18.8 MJ/kg for production, while metals like Au need 208.000 MJ/kg, and Rh needs 683.000 MJ/kg.[2] The energy required for other metals, as compared to Mg, is summarised in Fig. S16. Notably, Mg is one of the metals with the lowest energy demand for production. Magnesium electrolysis costs are further minimized by operating the process commercially at a large scale and hence the total energy required can be further reduced. Currently, Mg costs not more than 4 USD per kg [3] Recently, Mg was even produced for as low as ~1 USD per kg using a solar-energy pumped laser.[4]

In magnesium production, no CO_2 is released if the source is $MgCl_2$ or Mg-silicates. More excitingly, the entire Mg production process has one of the lowest impacts on global warming as compared to other metal catalysts for CO_2 reduction.[5] Magnesium produces 5.2 kg CO_2 per kg Mg, while metals like gold produce 12.500 kg CO_2 per kg Au, and rhodium produces 35000 kg CO_2 per kg Rh. CO_2 produced by other metals, as compared to Mg, is summarised in Fig. S17, indicating that Mg is one of the metals producing the lowest amount of CO_2 during production.

Thus, magnesium is the 8th most abundant metal, and costs only about $1.00 to 4.00 per kg. However, even being one of the cheapest metals, the cost of magnesium is still higher than that of the methane produced. However, the methane cost is low because currently, we get methane from natural sources. Methane is a greenhouse gas with 25 times more warming impact than CO_2, and ideally, methane should not be exposed to the environment, causing further damage. Since all the products (methane, methanol, formic acid and hydrogen) in this Mg process are produced from CO_2, it is an ideal CO_2 negative process. Thus, the price of these fuels can not be directly compared with that from current conventional processes (from fossil fuel or drilling natural methane). The idea of “cyclic economy” and “net-zero-emissions energy systems” is to use excess CO_2 by converting it to fuel (methane, methanol, formic acid, dimethyl ether (DME) etc) and then, after burning these fuels (to get energy), the CO_2 produced will again be captured and converted to fuel. This way, no CO_2 is released in the environment (CO_2 neutral process) and both of our problems of energy as well as global warming get resolved.

The LCA and cost calculations are tabulated below. This process is sustainable and economical, even without Mg regeneration.

Process	Energy (+ required or - produced)		CO_2 (+ released or - mitigated)
Electrolysis of Mg^{2+} to produce 1 Kg Mg	+ 0 MJ (Ideally + 18.8 MJ energy is required but was obtained from Solar Energy)		+ 0 kg (No CO_2 is released in the Mg production process when the source used is chloride or silicates.)
CO_2 conversion by 1 kg Mg	No external energy was required for this reaction	0 MJ	
	Product-Methane: Energy (50.1 kJ/g) released by burning 1.6 g of Methane	-0.0816 MJ	0.0044 kg (mitigated) 0.1 mol CO_2 converted to methane - 0.1 x 44 = 4.4 g
	Product-Methanol: Energy (22.7 kJ/g) released by burning 0.8138 g of Methanol	-0.0185 MJ	0.0011176 kg (mitigated) 0.0254 mol CO_2 converted to methanol -0.0254 x 44 = 1.1176 g
	Product-Formic Acid: Energy (6.4 MJ/lit) released by burning 0.98 mL of Formic Acid	-0.00627 MJ	0.001196kg (mitigated) 0.026 mol CO_2 converted to formic acid-0.026 x 46 = 1.196 g
	Product-Hydrogen: Energy (0.490 MJ/kg) required to produce 0.083kg hydrogen from fossil fuel (steam reforming of methane), which is saved by this process	-0.0406 MJ	- 0.76 kg (stopped from releasing to the environment) 9.21 kg CO_2 per kg H_2 emitted if produced from methane reforming, i.e. 0.76 kg CO_2 could have been emitted if H_2 was produced from methane.
	Energy (141.86 MJ/kg) released by burning 0.083 kg hydrogen	-11.77 MJ	0 kg (no emission)
	Product- Mg Basic Carbonate: Mg basic carbonate (heat of formation of carbonate)	-2.08 MJ	- 1.44 kg (mitigated) 1 kg Mg produced 3.85 kg basic carbonate by reacting with 1.44 kg CO_2
	Total	**11.91 MJ (Energy generated)**	**2.2 kg (CO_2 mitigated)**

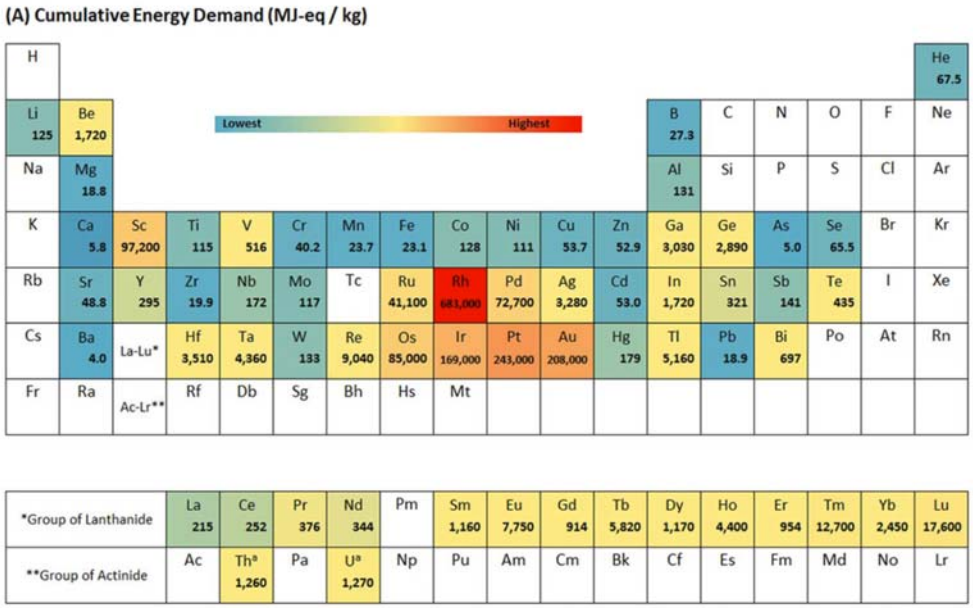

Figure S15. Cradle-to-gate cumulative energy demand (CED) (MJ-eq/kg) per kilogram of each element, including various metals used in CO_2 conversion. Reproduced from Ref. 5, Copyright PLOS.

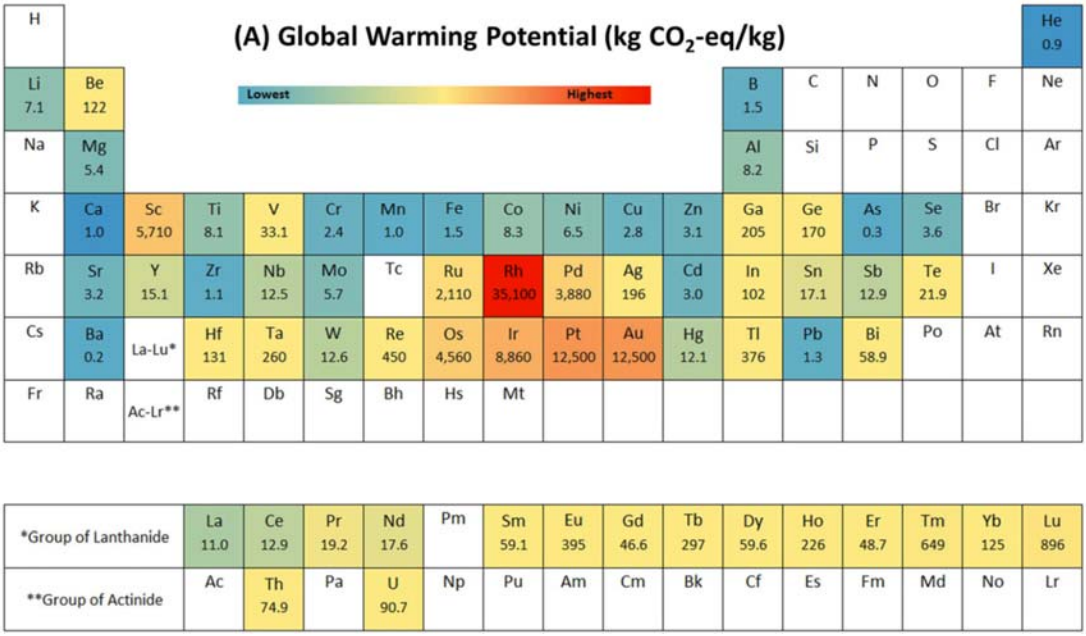

Figure S16. Global warming potential (CO_2 produced) per kilogram of each element, including various metals used in CO_2 conversion. Reproduced from Ref. 5, Copyright PLOS.

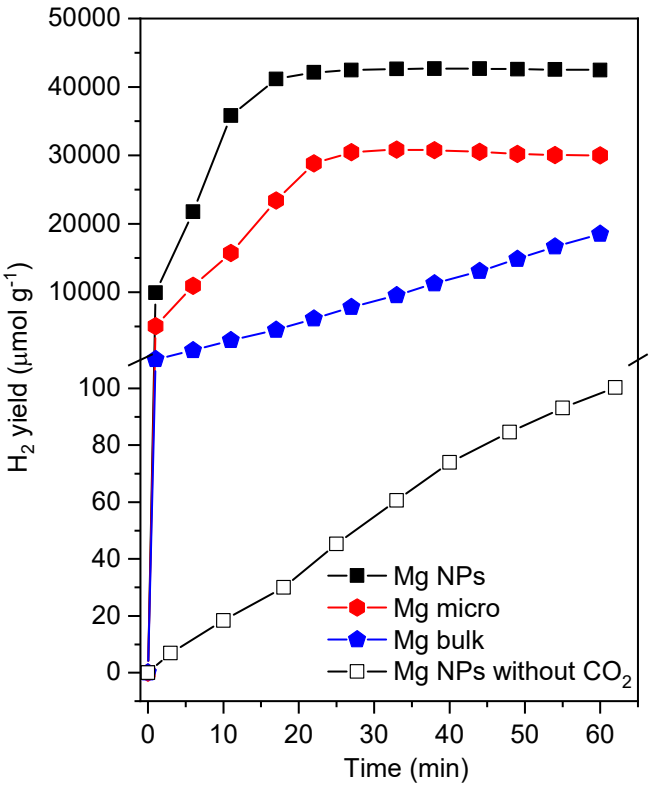

Figure S17. Hydrogen yield with reaction time during reduction of CO_2 at room temperature and ambient pressure. Notably, in the absence of CO_2, Mg does not react efficiently with water and hydrogen yield was extremely low, 100 µmol g^{-1} as compared to 42000 µmol g^{-1} in the presence of CO_2. This was due to poor solubility of magnesium hydroxide formed by reaction of Mg with water, restricting the internal Mg surface to react further with water. However, in the presence of CO_2, magnesium hydroxide gets converted to carbonates and basic carbonates, which are more soluble in water than magnesium hydroxide and gets peeled off from Mg, exposing fresh Mg surface to react with water. Thus, this protocol can even be used for hydrogen production (940 mL g^{-1}), which is nearly 420 times more than hydrogen produced by the reaction of Mg with water alone (2.24 mL g^{-1}).

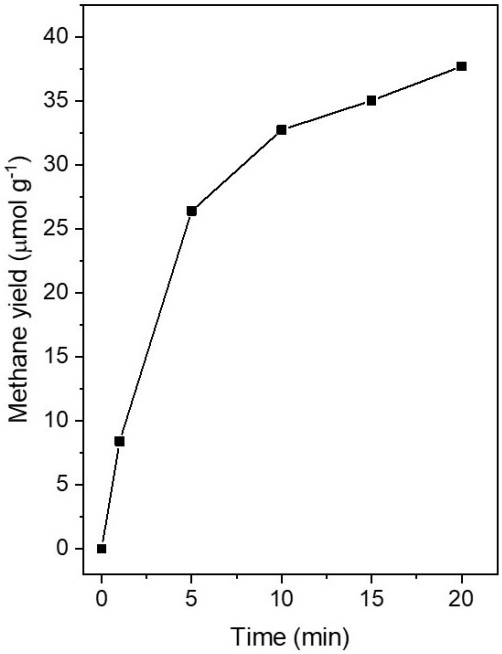

Figure S18. Methane yield with reaction time, for reduction of CO_2 in water using Mg NPs, at – 1 to +1 °C at atmospheric pressure.

Table S1. Elemental analysis of Mg NPs by SEM-EDX

Sample	Mg (wt%)	O (wt%)*
Mg NPs	80.06	19.94

* SEM-EDX is surface elemental techniques, indicating the presence of MgO layer on Mg NPs surface.

Table S2. Methanol, formic acid, and methane yield (normalized by Mg contents) for reduction of CO_2 using water at room temperature and atmospheric pressure in 1 h.

Sample Name	**Composition of sample**	**Composition (wt. %)**		**CH_4**	**Formic acid**	**Methanol**
		Mg	Metal	μmol/g of Mg	μmol/g of Mg	μmol/g of Mg
Mg_2Ni	Mg_2Ni	80	20	107	32	30
MgCa	$Ca_{0.06}Mg_{0.93}$	90	10	59	24	31
MgAl	$Al_{0.6}Mg_{0.4}$	62	38	87	35	34
Mg NPs	Mg	100	0	96	26	25
Mg bulk	Mg	100	0	16	15	17
Mg micro	Mg	100	0	78	23	31
MgH_2	MgH_2	100	0	0	4	3

Table S3. Contribution from different carbons with respect to the adventitious carbon at different time intervals.

Sample	Ratio of different species with respect to adventitious carbon			
	OCH_3	C-O	Carbonyl species (C=O)	Carbonate (CO_3^{2-})
Mg NPs	0	0.095	0.265	0.475
After 1 min	0.676	0	0.484	0.676
After 5 min	0.627	0	0.671	0.629
After 15 min	0.552	0	0.613	0.975

Table S4. Analysis of CO_2 activation via different proposed pathways.

Pathways	C-O bond length (Å)		OCO bond angle (°)	Charge transferred (Mg to CO_2) **Δq (e)**	CO_2 Binding Energy (eV)
I	1.22	1.19	140.80	0.17	-0.31
II	1.21	1.18	145.12	0.15	-0.28
III	1.19	1.17	155.34	0.11	0.42

Table S5. Different parameters of Mg surface adsorbed HCOOH, CH_3OH and CH_4 species.

Adsorbed Species	Observed distance (Å)	bonding distance (Å)	Reaction Energy (eV)
HCOOH	d(Mg-O) = 2.22	2.10	-0.26
CH_3OH	d(C-O) = 1.61	1.43	-0.32
CH_4	d(C-O) = 2.60	1.43	-0.68

Table S6. Methane production cost-comparison of Mg mediated process with various reported room temperature CO_2 conversion protocols.

S. No	**Metal (energy)**	**Methane Yield**	**Price of Metal**	**Methane Yield (per USD)**	**References**
1	Mg NPs (No external energy)	100 µmol g^{-1}	1$ per Kg	100000 µmol/$	This work
2	Au NPs (visible light)	0.63 µmol g^{-1}	45$ per g	0.014 µmol/$	6
3	Au Colloidosomes (visible light)	1.5 µmol g^{-1}	45$ per g	0.033 µmol/$	7
4	Pd_7Cu_1 (visible light)	19.6 µmol g^{-1}	50$ per g	0.392 µmol/$	8
5	Au-Co (visible light)	0.13 µmol g^{-1}	45$ per g	0.0029 µmol/$	9

References:

1. Polmear, I. J. *Magnesium and Magnesium Alloys*, Eds. M. M. Avedesian and H. Baker (ASM International, OH, USA, 1999, 3–6).

2. Nuss, P., Eckelman, M. J. Life Cycle Assessment of Metals: A Scientific Synthesis, *PLoS ONE* **9** e101298 (2014).

3. Demirci, G., Karakaya, I. *Magnesium Technology 2012*, Eds. Mathaudhu, S. N., Sillekens, W. H., Neelameggham, N. R., Hort N. (John Wiley & Sons, Hoboken, NJ, USA, 2012, 59–62).

4. Kostanyan R. K. Use of magnesium as renewable energy source. *Int. J. Chem. Mol. Eng.* **11**, 416-421 (2017).

5. Nuss, P., Eckelman, M. J. Life Cycle Assessment of Metals: A Scientific Synthesis. *PLoS ONE* **9,** e101298 (2014).

6. Yu, S., Wilson, A. J., Heo, J. Jain, P. K. Plasmonic control of multi-electron transfer and C-C coupling in visible-light-driven CO_2 reduction on Au nanoparticles. *Nano Lett.* **18**, 2189-2194 (2018).

7. Dhiman, M., Maity, A., Das, A., Belgamwar, R., Chalke, B., Lee, Y., Sim, K., Jwa-Min Nam, J.-W., Polshettiwar, V. Plasmonic colloidosomes of black gold for solar energy harvesting and hotspots directed catalysis for CO_2 to fuel conversion. *Chem. Sci.* 10, 6694-6603 (2019).

8. Long, R., Li, Y., Liu,Y., Chen, S., Zheng, X., Gao, C., He, C., Chen, N., Qi, Z., Song, L., Jiang, J., Zhu, J., Xiong, Y. Isolation of Cu atoms in Pd lattice: forming highly selective sites for photocatalytic conversion of CO_2 to CH_4. *J. Am. Chem. Soc.* **139**, 4486−4492 (2017).

9. Cui, X., Wang, J., Liu, B., Ling, S., Long, R., Xiong. Y., Turning Au nanoclusters catalytically active for visible-light-driven CO_2 reduction through bridging ligands. *J. Am. Chem. Soc.* **140**, 16514-16520 (2018).